Optically polarized ^{129}Xe NMR investigation of carbon nanotubes

Catherine F. M. Clewett
Department of Physics, Fort Hays State University, Hays, Kansas 67601, USA

Steven W. Morgan* and Brian Saam
Department of Physics, University of Utah, Salt Lake City, Utah 84112, USA

Tanja Pietraß
Department of Chemistry, New Mexico Tech, Socorro, New Mexico 87801, USA

(Received 5 September 2007; revised manuscript received 16 June 2008; published 1 December 2008)

We demonstrate the utility of optically polarized ^{129}Xe NMR in a convection cell for measuring the surface properties of materials. In particular, we show adsorption of xenon gas on oxidatively purified single- and multiwalled carbon nanotubes. The interaction between xenon and multiwalled nanotubes produced by chemical vapor deposition was stronger than that of single- or multiwalled nanotubes produced by carbon arc discharge. Xenon was observed in gas, liquid, and adsorbed phases. The large polarization and moderate pressures of xenon ($\sim$0.2 MPa) allowed resolution of multiple lines in both the gas and condensed phases of xenon in contact with carbon nanotubes. Xe gas exchanges with physisorbed xenon in two different environments. Xe adsorbs preferentially on defects, but if the number of defects is not sufficient, it will also adsorb on surface and interstitial sites. Penetration of Xe in the tube interior was not observed.

DOI: 10.1103/PhysRevB.78.235402 PACS number(s): 61.46.Fg, 32.80.Xx, 68.43.Fg, 68.43.−h

I. INTRODUCTION

Because of their unique electronic and mechanical properties, carbon nanotubes (CNTs) have been suggested for such applications as storage media and sensors for gases.[1] However, the sorption mechanism and uptake capacity of CNTs are still unclear.[2] Gas adsorption also affects their electronic structure. For instance, it has been shown that ammonia adsorbed on a nanotube makes a semiconducting nanotube metallic.[3] Experimental studies of gas adsorption on CNTs are most often done with macroscopic techniques such as thermal gravimetric analysis and temperature-programmed desorption which only indirectly probe the sorption mechanism.[2,4–6] Nuclear magnetic resonance (NMR) detection of adsorbates, however, can be used to identify adsorption sites, mechanisms, and strengths. Ripmeester and Davidson[7] and Ito and Fraissard[8] pioneered the use of ^{129}Xe as a probe for porous solids and surfaces exploiting xenon's large chemical shift range and chemical inertness. Prior work[9–11] showed that ^{129}Xe NMR is suitable for observing different adsorption sites in both single- and multiwalled nanotubes although it has been hampered by the presence of impurities and low signal-to-noise ratio due to the small gyromagnetic ratio of ^{129}Xe.

The interaction between ^{129}Xe and unpurified single- and multiwalled CNTs has previously been studied using NMR of naturally abundant xenon at pressures near 2 MPa.[9] The high pressures were necessary to increase the xenon spin density to such an extent that an NMR signal was observable. Overall, the adsorption was weak. Physisorption occurred at 198 K for unpurified multiwalled nanotubes and at 173 K for unpurified single-walled nanotubes. From the analysis of line widths, relaxation times, and integrated signal intensities, it was concluded that xenon adsorbed preferentially on the metal particles in single-walled nanotubes and on defect sites in multiwalled nanotubes. Spectral hole-burning experiments suggested a heterogeneity of adsorption sites, with highly mobile xenon on the surface of the CNTs. Xenon formed a bulklike phase with an estimated adsorption energy of 1.6 kJ/mol—a much lower adsorption energy than the 22.3 kJ/mol predicted for xenon monolayer adsorption[12] and much closer to the Xe-Xe attractive potential of 0.96 kJ/mol.[13] In ambient temperature studies at pressures $\sim$0.1 MPa, Romanenko *et al.*[10] were only able to observe the gas phase signal. Kneller *et al.*[11] used low temperatures and continuous-flow spin-exchange optical pumping (SEOP) of ^{129}Xe. Optical pumping enhances the sensitivity of the NMR experiment by up to 4 orders of magnitude.[14]

In this work, we use a spin-exchange convection cell[15] to optically polarize the xenon gas *in situ* with the sample (see Fig. 1). The convection cell allows xenon gas, continuously hyperpolarized in a closed steady-state convection loop, to come into contact with the CNT samples, with the entire apparatus in the 1.5 T field of a horizontal bore imaging magnet. Unlike typical implementations of flow-through xenon polarizers, the polarized gas stream contains a high xenon concentration (nearly 80%).

II. EXPERIMENTAL

A. Samples

One single-walled and two multiwalled CNT samples were obtained from Mer Corporation (Tucson, AZ) and were purified. Two of the as-produced samples have previously been studied with ^{129}Xe NMR,[9] while the purified samples have not. All of the samples, purified and as produced, have been characterized in previous work.[16] Surface area measurements were calculated from multipoint Brunauer-Emmett-Teller (BET) isotherms taken with N_2 gas at liquid N_2 tem-

TABLE I. Sample characteristics after oxidative purification (Ref. 16).

Sample	MRSW	MRGC	MRMWC
Production method	CAD[a]	CAD[a]	CVD[b]
Structure	Single walled Open	Multiwalled Closed	Multiwalled Open
Ave. tube diameter (nm)	1.5	18.2	81.9
Ave. bundle diameter (nm)	14	36	NA
Specific surface area (m^2/g)	10.4	29	26
Metallic catalyst	Co, Ni	None	Fe
ICP-MS (wt.%)[c]	15	0.3	3
Comments	Residual catalyst particles	Nano-onions	Damaged tube walls

[a]CAD=carbon arc discharge.
[b]CVD=chemical vapor deposition.
[c]ICP-MS is inductively coupled plasma–mass spectrometry. Data are given in $g_{\text{metal}}/g_{\text{raw material}} \times 100\%$.

peratures (77 K) using a Quantachrome Autosorb-MP1. Table I summarizes the sample characteristics. Each sample is referred to by the manufacturer's designation—MRSW and MRGC, single-walled and multiwalled nanotubes, respectively, produced by carbon arc discharge (CAD), and MRMWC, multiwalled nanotubes produced by chemical vapor deposition (CVD). MRGC is the only sample that was synthesized in the absence of any metal catalyst.

A two-stage purification procedure adopted from Dillon *et al.*[17] was used to remove impurities including graphitic material, amorphous carbon, and metallic catalyst. The samples were refluxed in 3 M HNO_3 for 16 h, filtered, and rinsed with deionized water until the filtrate was *p*H neutral. The sample was dried overnight and air oxidized at 833 K for 30 min. The harsh oxidation conditions also induced defects in some of the tubes. These particular samples are described in detail by Shen *et al.*[16]

B. SEOP convection cell and ^{129}Xe NMR

The sample retort of a xenon convection cell, similar to the one described by Su *et al.*,[15] was filled with purified CNTs. Each sample was sealed into its own cell with approximately 200 kPa Xe, 50 kPa He, and 8 kPa N_2 gas measured at room temperature; specific contents for each cell are shown in Table II. The convection cell was placed in a two-chambered housing consisting of an oven for the optical pumping sphere and a refrigerator for the sample region which also contained the NMR transmit or receive coil. The apparatus was placed in an Oxford horizontal-bore superconducting magnet with a field strength of 1.49 T. NMR studies were conducted with a TecMag Aries NMR spectrometer operating at the ^{129}Xe resonance frequency of 17.625 MHz. SEOP was performed with circularly polarized 795 nm light from a frequency-narrowed diode-laser array[18] collinear with the magnet bore. The sample was cooled with gas boiled from a liquid nitrogen reservoir and was temperature controlled between 163–273 K. Spectra were acquired using a low-angle pulse and signal averaging of up to 4096 scans. Use of the alternate NMR coil enclosing the gas retort, shown with a dashed line in Fig. 1, was used for the acquisition of pure gas phase xenon NMR spectra. Chemical shifts are referenced to the shift of gaseous xenon extrapolated to zero pressure at 273 K.[19]

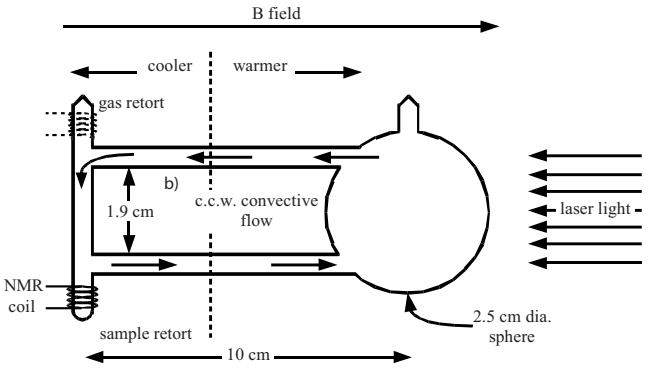

FIG. 1. Schematic drawing of the convection cell. The sample is located in the retort on the lower left, surrounded by the NMR coil. The cell is placed in a two-chambered housing, divided at the dotted line. The right half of the housing is maintained at 373 K; the left half of the housing is temperature controlled to the desired temperature between 163 and 273 K. The dashed lines on the gas retort show the alternate location for the NMR coil. Adapted with permission from Su *et al.* (Ref. 15)

III. RESULTS AND DISCUSSION

A. Sample morphology

Figure 2 shows the transmission electron micrographs (TEM) of each of the tubes, as characterized by Shen and

TABLE II. Convection cells used for experiments. Partial pressures of Xe, He, and N_2 (in kPa) at room temperature, mass of carbon nanotubes (mg), and total cell volume (cm^3) listed for each cell.

Sample	p_{Xe} (kPa)	p_{He} (kPa)	p_{N_2} (kPa)	Mass of CNTs (mg)	Cell vol. (cm^3)
MRSW	214.0	51.4	8.14	17.9	9.91
MRGC	205.0	51.6	8.03	45.7	10.68
MRMWC	196.0	53.4	8.19	22.6	10.67

Pietraß.[20] The single-walled sample, MRSW, consists of small diameter tubes (~1.5 nm) that form bundles with average diameter of 14 nm [Fig. 2(a)]. Purification caused opening of the tips of the tubes. Although purification removed some of the metallic catalyst material, inductively coupled plasma mass spectrometry (ICP-MS) still showed approximately 15(±1) wt % of the material to be cobalt and nickel catalysts. The tubes generally remained graphitized, and the size of the bundles decreased. The specific surface area of these purified tubes determined from the adsorption isotherms, 10.4 m^2/g, is much smaller than similar CAD tubes reported in the literature which had only been heat treated.[21] MRGC did not exhibit tube damage; the walls remained straight and the tips closed. The large particles evident in Fig. 2(b) are well graphitized carbon nano-onions with a mean diameter of 50 nm which are not attacked by the acid purification. The average diameter of the MRGC nanotubes was on the order of 18 nm. The TEM micrographs reveal a tendency for MRGC tubes to aggregate in small bundles of three or four nanotubes [Fig. 2(b)]. The interior of these nanotubes is not accessible to the xenon gas. The adsorption isotherm determined specific surface area is 29 m^2/g. On the other hand, MRMWC was damaged by purification. These CNTs also show signs of exfoliation of the outer layers, and the tubes were opened. Catalyst particles which were originally embedded in the tubular structure are removed in the purification leading to voids in the tube wall that may provide access to the tube interior. The diameter of the tubes is larger than that of the other samples: ~80 nm after purification. These tubes, however, do not bundle, and their specific surface area is 26 m^2/g, slightly larger than for other CVD multiwall nanotubes referenced by Migone and Talapatra.[21] The higher surface area could be accounted for by the tube damage and exfoliation.

By comparing the number of xenon atoms available in each of the cells (Table II) and using 18.03 A^2/atom as the specific area of Xe, we calculated the maximum number of monolayers of xenon that could be formed on the CNTs. Using the specific surface area of 10.4 m^2/g and a mass of 17.9 mg for MRSW there is enough gas to cover MRSW with 55 layers of Xe atoms. Similar calculations estimate seven layers for MRGC and 16 layers for MRMWC. Overall, these are thick layers compared to many other isotherm studies.[21]

TEM reveals multiple adsorption sites: defect sites at opened tube ends or tube walls, interstitial sites in tube bundles, the interior of open tubes, and residual metal particles. For MRGC, adsorption may also occur on the nano-onions.

B. Chemical shift and chemical exchange

Ratcliffe[22] characterized the NMR frequency shift δ_{obs} of ^{129}Xe on surfaces arising from the sum of various interactions

$$\delta_{obs} = \delta_0 + \delta_{Xe} + \delta_S + \delta_{SAS} + K + \delta_M, \quad (1)$$

where δ_0 is the reference shift. The shift due to Xe-Xe interactions δ_{Xe} is both pressure and temperature dependent. Confinement causes an increasingly downfield shift with decreasing pore size.[23] δ_{Xe} for free gas has been determined in the temperature range of 240–440 K for densities up to 250 amagat[24] and it is used here to determine the chemical shift of the gas phase not in contact with the carbon nanotubes.[19] The resonance frequency of free xenon gas appears near 0 ppm. Solid xenon, in the absence of other interactions, resonates near 300 ppm, and liquid xenon, appearing as a narrow peak, resonates near 240 ppm. δ_S is a term describing chemical shielding induced by the interaction of a single Xe with the atoms of the surface.[25] In most cases, the resonance from these atoms appears between the gas and solid lines. Strong adsorption sites should give rise to their own chemical shift δ_{SAS}. The xenon atoms at these sites, however, are not in exchange with the continuously provided freshly polarized gas and cannot be observed in our experiment. K is the Knight-shift contribution which originates from the Fermi contact interaction between an s-type conduction-electron

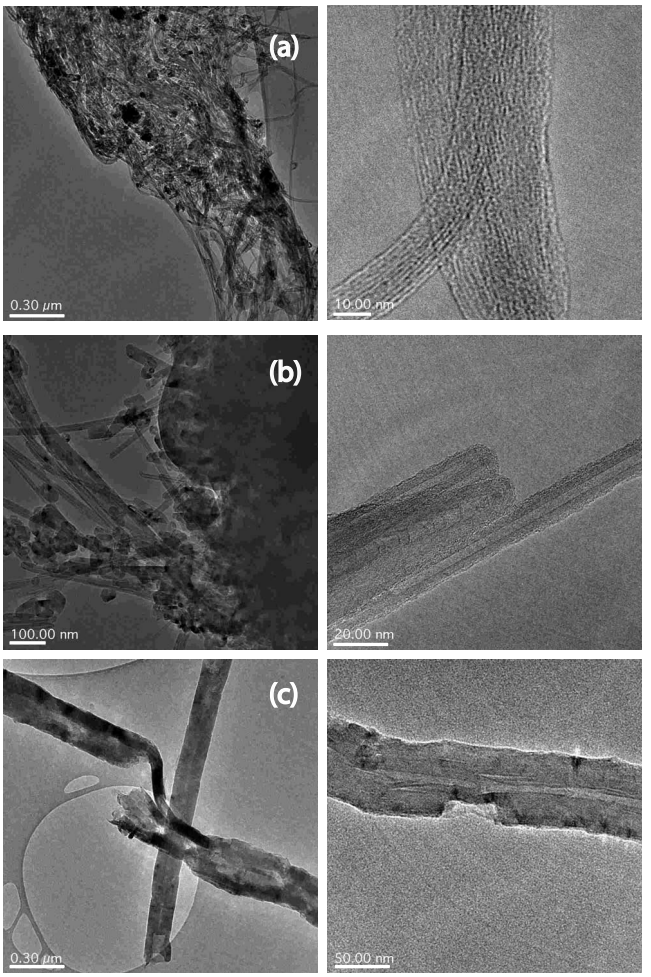

FIG. 2. TEM micrographs of the three samples at two magnifications. (a) MRSW: The dark particles are Ni- and Co-catalyst materials (left), and the tubes are bundled (right). (b) MRGC: At the lower magnification, the nanotubes are straight lines while the polyhedrons are nano-onions (left). Also notice the closed ends and bundling of the nanotubes (right). (c) MRMWC: Severe damage by the acid treatment opens the tubes (left) and introduces damage to the tube walls (right).

spin and the nuclear spin of the xenon atom. Finally, δ_M is a paramagnetic shift term due to the dipole-dipole interaction and it is on the order of 2000 ppm for Ni clusters in contact with xenon,[22] which is outside our frequency range. Xe experiencing a frequency shift due to paramagnetic sites will also be subject to fast relaxation,[26] and like xenon on strong adsorption sites, will not be visible in the spectrum. This is the same mechanism likely responsible for fast relaxation of optically polarized Xe gas in uncoated cells.[26] These paramagnetic sites, however, indirectly affect our spectra and will be explained further below.

The chemical shift in our situation can thus be simplified to

$$\delta_{\text{obs}} = \delta_{\text{Xe}} + \delta_S + K. \tag{2}$$

Physisorbed xenon spans the range from 0–300 ppm,[22] and the temperature dependence of the shift is a measure of the strength of the interaction. For weakly interacting particles, the adsorbed phase signal only becomes observable at lower temperatures.

When a xenon atom moves between inequivalent sites (in this case between the gas phase denoted by frequency ω_A and an adsorption site denoted by frequency ω_B), its magnetic environment changes and its frequency shifts. This effect is known as chemical exchange. In order to determine the effect on the spectrum, it is necessary to compare the rate of motion of the atom R_{hop} with the frequency shift difference $\Delta\omega = \omega_A - \omega_B$ of the NMR lines corresponding to those sites. Following the analysis of Pople *et al.*,[27] in the slow exchange limit $R_{\text{hop}} \ll \Delta\omega$, the two lines will be resolved, while in the fast exchange limit $R_{\text{hop}} \gg \Delta\omega$, the frequency of the two lines is averaged. If $R_{\text{hop}} \leq \Delta\omega$, then the two lines are broadened with maximum line width occurring at $R_{\text{hop}} = \Delta\omega/\sqrt{2}$. The average line position (or frequency) is based on the population at each site. If the spin-lattice relaxation times T_1 are similar for each site, then the averaged signal will appear somewhere between the two frequencies corresponding to each individual site. If however, the relaxation time is shorter at one of the two sites, the nonequilibrium polarization of the spin is destroyed at this site and becomes unobservable. In this case, only line broadening may give evidence of exchange. In our case, xenon moving between an adsorption site and the gas phase, the T_1 s are different by orders of magnitude. T_1 for free xenon gas is on the order of 10^3 s, while relaxation due to the unpaired electronic spin of a paramagnetic site can be as short as 10^{-9} s.[26] Therefore, the contribution from any spin that samples a paramagnetic site will not appear in the spectrum.

^{129}Xe NMR spectra at selected temperatures are shown in Fig. 3 for each of the samples and are compared to the gas signal at 273 K. Spectra were recorded at 163 K and in the range 173–273 K in steps of 20 K. At applied pressures, gas and liquid xenon coexist at temperatures of 173 K and below and the signal for liquid xenon near 240 ppm is expected in each of the cells; however, it was observed neither in the previous work with P_{Xe} near 2 MPa (Ref. 9) nor in the present work. Here, liquid xenon relaxes too fast for NMR observation due to its lower mobility than the gas phase and intimate contact with paramagnetic sites. The only sample that gives direct evidence of an adsorbed phase in this work is the MRGC sample (~260 ppm), even though both of the other samples (MRSW and MRMWC) displayed adsorption signals near 250 ppm in the high-pressure studies.[9]

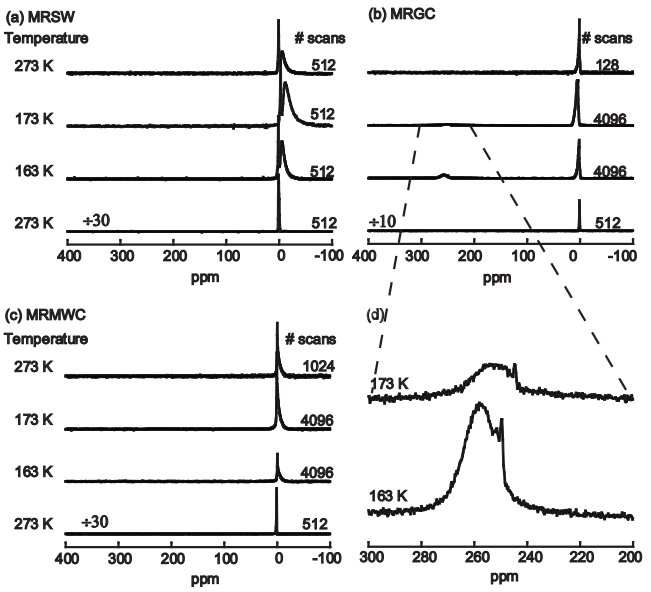

FIG. 3. ^{129}Xe spectra of xenon in convection cells in close contact with carbon nanotubes at three temperatures: 273, 173, and 163 K. The bottom spectrum for each sample is the spectrum for the gas at 273 K recorded with the alternate NMR coil (see Fig. 1). Signal intensities have been scaled to account for the different number of scans used at each temperature, resulting in different noise levels. The number of scans for each spectrum is listed to the right. For ease of view, the gas signal has been reduced by the factor shown. The relaxation delay was based on the time for the convection cycle, 1 s. (a) MRSW, (b) MRGC, (c) MRMWC, and (d) MRGC adsorbed phase. Notice that the MRGC sample is the only one to show adsorbed peaks, ~260 ppm, due to the low density of paramagnetic defect sites.

C. Signal intensity

At the pressures used in this work, a larger percentage of the xenon atoms interacts directly with the surface of the CNTs than at higher pressure.[9] Xenon atoms moving sufficiently close to the surface to relax completely through paramagnetic interactions with catalyst particles or defects become unobservable to NMR. Nevertheless, the effect of the CNTs on xenon is noticeable through an analysis of the integrated signal intensities. Figure 4 shows the ratio of $I_{\text{CNT}}/I_{\text{gas}}$. I_{CNT} is the integrated signal intensity of the entire spectral range (−100–400 ppm) in the presence of CNTs (from Fig. 3). I_{gas} is the equivalent integrated signal intensity of xenon in the absence of CNTs at the same temperature (bottom spectra in Fig. 3). Both spectra were acquired under the same conditions—the only difference changing the position of the NMR coil to surround the gas retort. The ratio $I_{\text{CNT}}/I_{\text{gas}}$ is less than 1 if the exposure of the xenon gas to the CNTs destroys the xenon nuclear-spin polarization and causes a loss in NMR signal intensity.

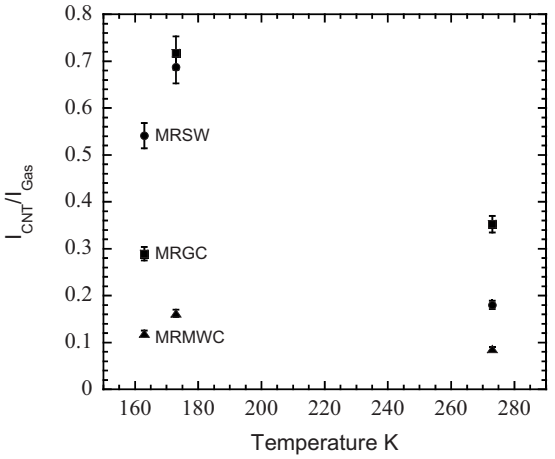

FIG. 4. Ratio for xenon gas signal intensity in contact with CNTs over the signal intensity of the free gas for each of the samples at three different temperatures. MRSW is shown as circles, MRGC as squares, and MRMWC as triangles. The signal intensity ratio is a function of the strength of interaction between xenon and the nanotubes. MRMWC with the lowest signal intensity ratio has the strongest interaction at all temperatures.

At high temperature, the kinetic energy of the gas allows polarized xenon to exchange easily with the xenon adsorbed on the CNTs. When the freshly polarized xenon samples paramagnetic sites on the CNTs the polarization is destroyed, reducing the overall signal intensity. We expect to see a reduction in signal intensity proportional to the density of paramagnetic sites in the CNTs. According to electron-spin resonance (ESR) results,[28] the samples have increasing numbers of defect sites in the order MRGC, MRSW, and MRMWC. MRGC has the fewest paramagnetic sites and retains the most polarization at 273 K, while MRMWC has the most paramagnetic sites and retains the least polarization (Fig. 4).

As the temperature is reduced to 173 K, relaxation slows because the mobility of the gas phase xenon is reduced while the convection velocity—the rate of replenishment of polarized gas—remains the same. At this temperature the retained signal is essentially equal for MRSW and MRGC. This implies that the xenon is exposed to an equivalent surface density of paramagnetic sites on the two samples. Intuitively, this similar surface density is understandable in that MRSW has a higher density of defect sites than MRGC, but it also has a smaller surface area and more layers of xenon atoms between the nanotube and the refreshed gaseous xenon. Therefore, the average distance to a paramagnetic site may be the same for the two samples.

At the coldest temperatures the kinetic energy of the xenon cannot overcome the adsorption potential of the nanotubes and the defect sites are assumed to be saturated from the multilayer adsorption. The adsorbed xenon cannot easily exchange with freshly polarized gas. For MRGC and MRSW, there is a significant change in signal intensity retained at the lower temperatures. Notice that for MRMWC there is essentially no change in the reported signal intensity ratio with temperature. Previous high-pressure work[9] demonstrated that xenon has a stronger interaction with the MRMWC nanotubes than with MRSW, which is confirmed

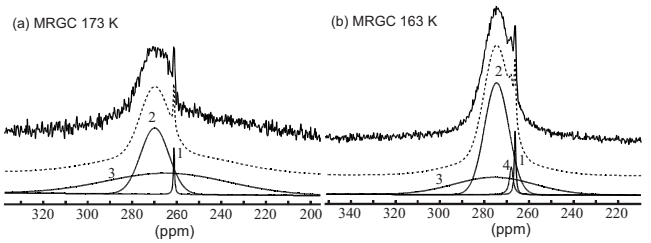

FIG. 5. ^{129}Xe NMR spectra of the adsorbed phase of MRGC at (a) 173 K and (b) 163 K. At 173 K the spectrum can be decomposed into 1 Lorentzian (1) and 2 Gaussian lines (2 and 3), while at 163 K, the spectrum is best fit with 2 Lorentzian (1 and 4) and 2 Gaussian lines (2 and 3). The experimental spectrum is shown at the top, the component lines on the bottom, and the sum of the components is the dashed line in the center.

in Fig. 4—I_{CNT}/I_{gas} is always smallest for the MRMWC sample. Also from the estimated xenon coverage, the interaction with the xenon is stronger for MRMWC than MRSW because of the larger surface area. We thus conclude that the adsorption potential for MRMWC is always greater than the kinetic energy available.

In summary, we can conclude from the signal intensity ratios in Fig. 4 that MRMWC has the strongest adsorption potential, which can be estimated to be between 2.2 and 3.4 kJ/mole from the thermal energy depending on the temperature used.

D. Adsorbed phase

A resonance for physisorbed xenon (about 260 ppm at 173 K) is only observed for MRGC: the multiwalled nanotubes made without catalyst and which ESR data[28] show have the fewest paramagnetic defect sites. The adsorbed phase resonance shifts downfield with decreasing temperature and gains intensity. Figure 5 shows the decomposition of this resonance using the program DMFIT.[29] At 173 K the spectrum is best fit with three lines—a narrow (11.5 Hz full width at half maximum) Lorentzian line at 245 ppm labeled 1 and two broad Gaussian lines labeled 2 and 3. It should be noted that at 173 K and 205 kPa gas and liquid phases should coexist.[30] The Lorentzian shape of line 1 suggests motional narrowing and is thus assigned to liquid xenon. All three lines move downfield with decreasing temperature, and a fourth line is observed at 163 K (Fig. 5). This line is also Lorentzian, width 35 Hz, appearing 1.72 ppm downfield from line 1. Because of its Lorentzian shape, line 4 is also assigned to more mobile xenon and its downfield shift suggests that it is due to more densely packed xenon in an enclosed space. Because lines 1 and 4 can be partially resolved at 163 K, the exchange rate appears to be in the intermediate regime where $R_{hop} \leq \Delta\omega$. From the frequency shift, the upper limit of the lifetime of the xenon at line 4 is $\tau = 0.002$ s. Since the MRGC tubes remain closed after purification and MRGC is nearly defect free, this leaves three possible sites for the adsorbed xenon: the outer grooved surface of the nanotube bundles, the interstitial sites in the bundles, and the outer surface of the nano-onions. Line 4 can also be partially resolved with lines 2 and 3, implying that line 4 is also in

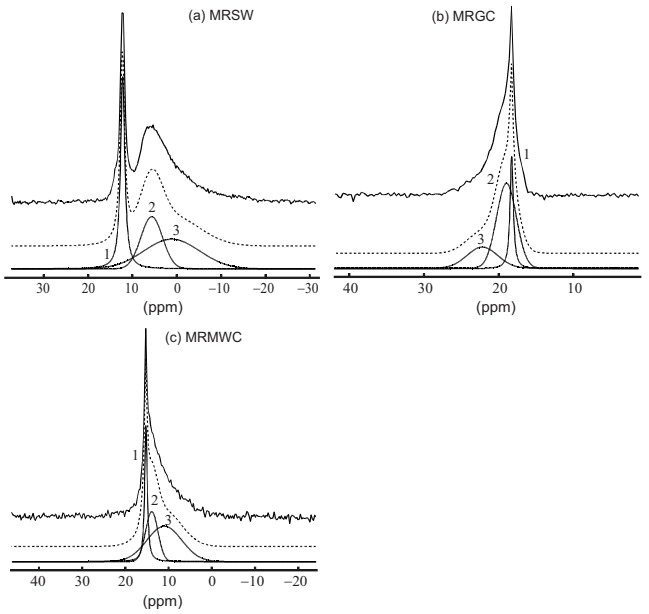

FIG. 6. ^{129}Xe NMR spectra of the gas phase for each of the samples at 273 K. Each spectrum can be decomposed into three lines: 1 Lorentzian (1) and 2 Gaussian (2 and 3). The experimental spectrum is shown at the top, the component lines on the bottom, and the sum of the components is the dashed line in the center. (a) MRSW. (b) MRGC. (c) MRMWC.

exchange with the adsorbed phase lines 2 and 3. Lines 2 and 3 are assigned to physisorbed xenon in two different environments. The Gaussian shape suggests that there is a heterogeneity of sites with less mobile xenon atoms. Both of these environments would be accessible to exchange with liquid xenon at the surface or in interstitial sites (lines 1 and 4) as is expected from the overlap of the signals at 163 K. Therefore, it can be concluded that the upper limit of the lifetime of xenon in the adsorbed phase is also τ=0.002 s. The measured relaxation time for xenon in the gas and adsorbed phase, however, is 2 orders of magnitude greater than this value of τ,[9] which implies that the adsorption/desorption of xenon is not the dominant relaxation mechanism for the gas. Instead, it confirms that relaxation to paramagnetic sites is much more efficient.

E. Gas phase

While MRGC displays two sets of resonances at distinctly different chemical shifts (0 ppm, ~260 ppm), MRSW and MRMWC display only a composite resonance close to 0 ppm. These resonances have a complex structure. Figure 6 shows the decomposition of the gas phase spectrum for each of the samples into three lines: a Lorentzian line (1) and two Gaussian lines (2 and 3). Line 1 stems from the free gas in the interparticle space; within error, it has the same width and line shape as the pure gas phase peak at all temperatures. The most striking feature of Fig. 6 is the negative chemical shift for lines 2 and 3 in MRSW and MRMWC. Negative xenon shifts have been reported previously in the literature.[22] Romanenko *et al.*[10] reported a negative shift for xenon in contact with single-walled nanotubes produced by methane decomposition over Ni- and Co-containing catalysts. Negative Knight shifts on the order of 1 to tens of parts per million have been observed and calculated for xenon in contact with metallic nanotubes[31] and metallic particles.[22] Since MRGC shows only positive chemical shifts and is the only sample that does not contain metallic particles, we conclude that the negative shifts are most likely due to interaction of xenon with metallic particles and not metallic CNTs—all samples should contain roughly the same fraction of metallic tubes. Therefore, we ascribe the negative shifts to Knight shifts due to interaction of xenon gas with metallic particles. The shift difference between line 1 and lines 2 and 3 is about 5 ppm for the MRMWC sample and is larger, 10–14 ppm, for the MRSW sample.

The Gaussian shape for lines 2 and 3 suggests a phase where xenon has limited mobility. This phase is not directly detected due to paramagnetic relaxation, and the frequency where it is observed depends on the exchange rate between the gas and the unobserved adsorbed phase. For rapid exchange,[27]

$$\omega_{\text{average}} = p_A\omega_A + p_B\omega_B, \tag{3}$$

where ω_A and ω_B are the frequencies of the xenon atoms at the two sites, in our case, the gas and the adsorbed phases, respectively. The weighting factors p_A and p_B are the fractional populations of the two sites. Usually, p_A and p_B are dependent on the lifetime at each site τ_A and τ_B, but in our case, the lifetime at site B is very short due to relaxation to paramagnetic sites $T_{1B} \approx 10$ ns,[26] and the weighting factors become[27]

$$p_A = \frac{\tau_A}{\tau_A + T_{1B}} \simeq 1 \quad \text{and} \quad p_B = \frac{T_{1B}}{\tau_A + T_{1B}} \simeq 0. \tag{4}$$

The averaged frequency thus appears much closer to the gas phase frequency ω_A. Lines 2 and 3 thus arise from heterogeneous adsorption sites of two different average environments in exchange with free gas. In accordance with the results for the adsorbed phase, we tentatively assign these two lines for MRGC and MRSW to the exterior of the bundles and the interstitial sites. Figure 7 shows a schematic representation of the adsorption sites available on each of the samples. Since the chemical shift of xenon is inversely proportional to the size of a confining pore,[23,32] line 3 with the largest chemical shift is assigned to xenon in interstitial sites. For MRMWC, interstitial sites are not available and restricted pores such as those shown in Fig. 2(c) or depicted in Fig. 7(c) may be occupied. For all three samples, line 2 is assigned to xenon on the outside surface of the nanotubes or bundles. This assignment is corroborated by the line width data (see Fig. 8). For all three samples, the width of line 2 (squares) is independent of temperature. MRGC and MRMWC have similar surface areas of 29 and 26 m^2/g, respectively. The width of line 2 for both samples is about 60 Hz. The smaller diameter of the single-walled nanotubes causes more corrugation to the outer surface of the bundle, corresponding to a greater heterogeneity of adsorption sites as shown in Fig. 7(a). MRSW is not shown in Fig. 8; how-

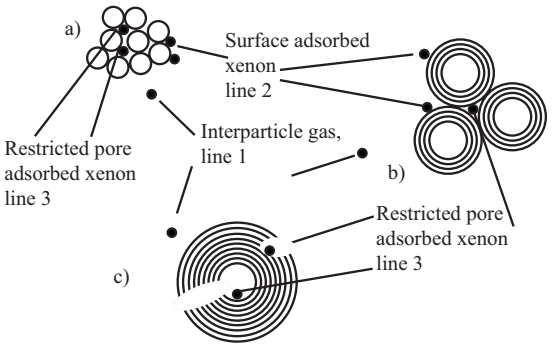

FIG. 7. Schematic representation of the adsorbed phases and interparticle gas for (a) MRSW, (b) MRGC, and (c) MRMWC. The small filled circles are ^{129}Xe. Line 1 in the spectra is assigned to interparticle gas, line 2 to gas on the surface of the carbon nanotubes, and line 3 to the more confined interstitial sites, defect sites, or interiors of multiwalled nanotubes (c).

ever, the width of line 2 for MRSW is correspondingly wider at ~100 Hz.

As temperature is decreased, line 3 (circles) broadens until 213 K for MRMWC and 173 K for both MRSW (not shown) and MRGC (Fig. 8). At lower temperatures, the line narrows. For MRGC, where the adsorbed phase is observable, the temperature for the maximum in-line width corresponds to the appearance of the resonance near 260 ppm for the adsorbed phase. The formation of an adsorbed phase depletes other adsorption sites, leading to a narrowing in the line width due to a reduced heterogeneity. The same phenomenon was observed at higher pressure.[9] Even though the adsorbed signal is unobservable for MRSW and MRMWC, the maximum in linewidth suggests that adsorption begins to occur at 213 K for MRMWC and 173 K for MRSW.

IV. CONCLUSIONS

We have studied xenon adsorption on single-walled and multiwalled, oxidatively purified carbon nanotubes using optically polarized ^{129}Xe NMR spectroscopy. We have demonstrated the utility of an optically polarized ^{129}Xe convection cell that continuously polarizes the xenon gas for measuring surface properties of materials. Because of the high polarization and the low pressures, multiple lines in both the gas and adsorbed phases of xenon in contact with CNTs can be resolved. Correlation with calculated and experimental adsorption isotherm data allows us to conclude that the xenon is highly mobile between multiple physisorbed sites on the surface. We propose these to be the outer surface of the carbon nanotubes and a second site which is dependent on the production method of the carbon nanotubes. For carbon arc discharge produced nanotubes, the second site is attributed to grooves on the exterior or interstitial sites in tube bundles.

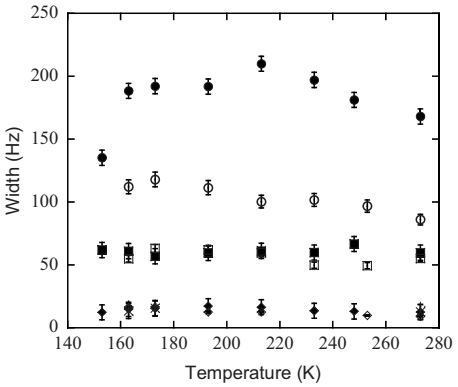

FIG. 8. Plot of linewidth vs temperature for MRMWC (filled symbols) and MRGC (open symbols). Gas phase line 1, diamonds, Gaussian line 2, squares, and Gaussian line 3, circles. The width of the line of gas not in contact with carbon nanotubes is denoted by plusses for MRMWC and crosses for MRGC. Notice that lines 1 and 2 are constant in width within error. The linewidth of line 3 increases with decreasing temperature to the onset of adsorption (213 K for MRMWC, 173 K for MRGC) then begins to narrow.

With decreasing temperature, this line continues to broaden until adsorption sets in and then narrows, demonstrating the slower exchange rate between these sites and the interparticle gas. For the chemical vapor deposition produced nanotubes, the second site is attributed to defects introduced in the oxidative purification procedure. Through the loss of polarization by relaxation to paramagnetic sites as well as through the presence of Knight shifts, we confirm that xenon adsorption occurs near defect sites in multiwalled nanotubes and metallic particles in single-walled nanotubes. We also show that, in general, adsorption seems to be stronger on the multiwalled nanotubes than the single-walled tubes in agreement with previous work.[9] The temperature-dependent spectra and the integrated signal intensities confirm that the adsorption potential of chemical vapor deposition produced multiwalled nanotubes (MRMWC) is stronger than that of either the single-walled tubes (MRSW) or the carbon arc discharge produced multiwalled nanotubes (MRGC).

ACKNOWLEDGMENTS

The authors would like to thank Danny Ferraro, Dylan Merrigan, and Jestina Hansen for assistance with purifying the nanotubes, Kai Shen for the TEM micrographs, and Kevin Teaford for manufacturing the sample cells. This work was funded in part by a research grant from the Vice Presidents for Research and Economic Development and Academic Affairs at New Mexico Tech and by the National Science Foundation (Grants No. PHY-0134980 and No. CHE-0107710).

*Present address: Department of Physics, Princeton University, Princeton, New Jersey 08544, USA.

[1] S. B. Sinnott and R. Andrews, Crit. Rev. Solid State Mater. Sci. **26**, 145 (2001).
[2] T. Pietraß, in *Handbook of Modern Magnetic Resonance*, edited by M. Utz (Springer-Verlag, New York, 2006), pp. 1459–1465.
[3] J. Kong, N. R. Franklin, C. Zhou, M. G. Chapline, S. Peng, K. Cho, and H. Dai, Science **287**, 622 (2000).
[4] A. C. Dillon and M. J. Heben, Appl. Phys. A: Mater. Sci. Process. **72**, 133 (2001).
[5] H. M. Cheng, Q. H. Yang, and C. Liu, Carbon **39**, 1447 (2001).
[6] R. G. Ding, G. Q. Lu, Z. F. Yan, and M. A. Wilson, J. Nanosci. Nanotechnol. **1**, 7 (2001).
[7] J. A. Ripmeester and D. Davidson, J. Mol. Struct. **75**, 67 (1981).
[8] T. Ito and J. Fraissard, J. Phys. Chem. **76**, 5225 (1982).
[9] C. F. M. Clewett and T. Pietraß, J. Phys. Chem. B **109**, 17907 (2005).
[10] K. V. Romanenko, J. B. D. de la Caillerie, J. Fraissard, T. V. Reshetenko, and O. B. Lapina, Microporous Mesoporous Mater. **81**, 41 (2005).
[11] J. M. Kneller, R. J. Soto, S. E. Surber, J.-F. Colomer, A. Fonseca, J. B. Nagy, G. Van Tendeloo, and T. Pietraß, J. Am. Chem. Soc. **122**, 10591 (2000).
[12] A. Šiber, Phys. Rev. B **68**, 033406 (2003).
[13] B. Lehner, M. Hohage, and P. Zeppenfeld, Phys. Rev. B **65**, 165407 (2002).
[14] T. G. Walker and W. Happer, Rev. Mod. Phys. **69**, 629 (1997).
[15] T. Su, G. L. Samuelson, S. W. Morgan, G. Laicher, and B. Saam, Appl. Phys. Lett. **85**, 2429 (2004).
[16] K. Shen, H. F. Xu, Y. B. Jiang, and T. Pietraß, Carbon **42**, 2315 (2004).
[17] A. C. Dillon, T. Gennett, K. M. Jones, J. L. Alleman, P. A. Parilla, and M. J. Heben, Adv. Mater. (Weinheim, Ger.) **11**, 1354 (1999).
[18] B. Chann, I. Nelson, and T. G. Walker, Opt. Lett. **25**, 1352 (2000).
[19] C. Jameson, A. Jameson, and S. Cohen, J. Chem. Phys. **59**, 4540 (1973).
[20] K. Shen and T. Pietraß, J. Phys. Chem. B **108**, 9937 (2004).
[21] A. D. Migone and S. Talapatra, *Encyclopedia of Nanoscience and Nanotechnology* (American Scientific, New York, 2004), Vol. 3, pp. 749–767.
[22] C. I. Ratcliffe, *Annual Reports on NMR Spectroscopy* (Academic, San Diego, 1998).
[23] J. Ripmeester, C. Ratcliffe, and J. Tse, J. Chem. Soc., Faraday Trans. 1 **84**, 3731 (1988).
[24] The density of an ideal gas at STP is 1 amagat=2.69 $\times 10^{19}$ cm^{-3}.
[25] A. C. de Dios and C. J. Jameson, in *Annual Reports on NMR Spectroscopy*, edited by G. A. Webb (Academic, London, 1994), Vol. 3, pp. 1–69.
[26] B. Driehuys, G. D. Cates, and W. Happer, Phys. Rev. Lett. **74**, 4943 (1995).
[27] J. A. Pople, W. G. Schneider, and H. J. Bernstein, *High-Resolution Nuclear Magnetic Resonance* (McGraw-Hill, New York, 1959).
[28] K. Shen, D. L. Tierney, and T. Peitrass, Phys. Rev. B **68**, 165418 (2003).
[29] D. Massiot, F. Fayon, M. Capron, I. King, S. Le Calve, B. Alonso, J. Durand, B. Bujoli, Z. Gan, and G. Hoatson, Magn. Reson. Chem. **40**, 70 (2002).
[30] V. A. Rabinovich, A. A. Vasserman, V. I. Nedostup, and L. S. Veksler, *Thermophysical Properties of Neon, Argon, Krypton, and Xenon* (Hemisphere, Washington, 1988).
[31] O. V. Yazyev and L. Helm, Phys. Rev. B **72**, 245416 (2005).
[32] T. Cheung, J. Phys. Chem. **96**, 5505 (1992).